Eur. Phys. J. D **24**, 335–338 (2003)
DOI: 10.1140/epjd/e2003-00168-7

THE EUROPEAN PHYSICAL JOURNAL D

Structures and reactions of biomolecular ions produced with electrospray ionization

S. Nonose[a], S. Iwaoka, H. Tanaka, N. Okai, T. Shibakusa, and K. Fuke

Department of Chemistry, Faculty of Science, Kobe University, Kobe 657-8501, Japan

Received 10 September 2002
Published online 3 July 2003 –

Abstract. Photo-induced reaction of [Fe(III)-protoporphyrin]$^+$ (hemin$^+$) ions solvated with dimethylsulfoxide (DMSO) is investigated by using a tandem mass spectrometer with electrospray ionization. We measure the photodissociation yields of mass-selected hemin$^+$(DMSO)$_n$ clusters for $n = 0-3$. The mass spectra of the fragment ions show the β-cleavage of carboxymethyl groups in addition to the evaporation of solvent molecules. Yield of the β-cleavage reaction is found to depend strongly on the excitation energy and the number of solvent molecules. We also examine photo-induced reactions of multiply-charged cytochrome c ions, $(M + nH)^{n+}$ ($n = 9-17$). Photoionization is found to be the dominant process for the lower charged states ($n = 9-12$) and its yield decreases rapidly with increasing the charge. The photoionization is ascribed to the emission of electron by multiphoton excitation of heme under the influence of Coulomb attractive potential arising from the charges in the polypeptide chain. Model calculations of the Coulomb potential suggest that the structure of the polypeptide chain is completely elongated.

PACS. 36.40.-c Atomic and molecular clusters – 71.22.-f Electronic structure of nanoscale materials: clusters, nanoparticles, nanotubes, and nanocrystals

1 Introduction

Clusters bridge the gap between the gas phase and the condensed phase. Structures and reactions of gas-phase clusters have been studied extensively using various spectroscopic methods [1]. For examples, the electronic structures of the clusters such as metal atoms and/or ions solvated with polar molecules have been investigated for modeling microscopic solvation [2–4]. Recent advances in electrospray ionization (ESI) allow us to produce various kinds of nonvolatile molecules in the gas phase without destruction [5]. Several groups have applied ESI to the spectroscopic studies of the gas-phase cluster ions [6–8].

Metalloporphyrins are active sites of numerous proteins whose functions range from oxygen transport and storage to electron transport and energy conversion [9]. The chemical reactivity and reaction dynamics of metalloporphyrins and heme proteins in condensed phase are strongly influenced by the surrounding solvent environments. In order to investigate the microscopic solvation and the dynamics of reaction, they are introduced into the gas phase as ions. The gas phase is an unusual environment for the investigation of these biological molecules. However, the gas-phase studies are expected to provide a deeper understanding of the intramolecular interactions as well as solvation interactions that determine the structures and reactions. Several different techniques have been employed to obtain information on the structures and reactions of biological molecules in the gas phase [10–13].

In the present work, the photo-induced reaction of dimethylsulfoxide (DMSO) clusters containing [Fe(III)-protoporphyrin]$^+$ (hemin$^+$) ions are investigated in order to clarify the mechanism of the β-cleavage reaction. Because the dipole moment of DMSO (2.54 Debye) is much larger than that of water, DMSO strongly interacts with ionic species in the gas phase as well as in the solution. Therefore, an extensive solvation effect would be expected for the reactions of DMSO clusters containing hemin$^+$ ion. The photodissociation yields at 28200 and 18800 cm^{-1} for mass-selected hemin$^+$(DMSO)$_n$ clusters ($n = 0-3$) are examined. In order to understand the microscopic interactions of heme with polypeptide chains in the gas phase, we also study the photo-induced reactions of multiply-charged cytochrome c ions. Cytochrome c is a relatively small protein and has an iron-containing heme group covalently bound to two cysteines in a polypeptide chain of ∼100 residues. We measure the photoionization yields at 28200 and 18800 cm^{-1} for the charge-selected cytochrome c ions, $(M + nH)^{n+}$ ($n = 9-17$). Based on these results, we discuss the mechanisms of the photoionization and photodissociation of heme in relation to the protein conformations.

[a] e-mail: nonose@kobe-u.ac.jp

2 Experimental

Details of the experimental apparatus used in the present study have been described elsewhere [14,15]. Briefly, the system consists of an ESI source and a tandem mass spectrometer with octapole ion beam guides. Hemin$^+$(DMSO)$_n$ ions are produced by ESI of a dilute solution of Fe(III)-protoporphyrin chloride in methanol-dichloromethane (1:1 v/v) mixture including dimethylsulfoxide (DMSO) (1.0%). Multiply-charged protein ions are produced by ESI of a dilute solution of cytochrome c in methanol-water (1:1 v/v) mixture including acetic acid (2.0%). The electrospray needle is biased at 4.5−5.0 kV with respect to a platinum aperture of 0.1 mm in diameter. A flow of 10−800 ml/s of dry nitrogen is maintained through the atmospheric pressure ion source. Ions formed in the ESI source are admitted into the first vacuum chamber. The ion beam is then pass through a stainless-steel skimmer, and is focused by electrostatic lenses into the first octapole-ion-beam guide (OPIG1). The OPIG1 is connected directly to the first quadrupole mass spectrometer (QMASS1) in the second chamber. The mass-selected ions emerging from the QMASS1 are deflected 90° by a first quadrupole ion deflector, and are admitted into the second octapole-ion-beam guide (OPIG2) in the third chamber. High transmission efficiency for slow ions is accomplished by applying a radio frequency (RF) field to the OPIGs. After passing through OPIG2, the parent and product ions are deflected 90° by the second quadrupole ion deflector, and are admitted into the second quadrupole mass spectrometer (QMASS2). The ions are detected by a channeltron electron multiplier equipped with a conversion dynode. Signals from the detector are fed into a current amplifier and are averaged by a digital storage oscilloscope. Depletion yield of the parent cluster ions in OPIG2 is measured with irradiating a photolysis laser. The laser beam is introduced into the guide collinearly and counterpropergatedly with the ion beams. We use the second (18800 cm^{-1}) or third (28200 cm^{-1}) harmonic of a YAG laser as the photolysis laser.

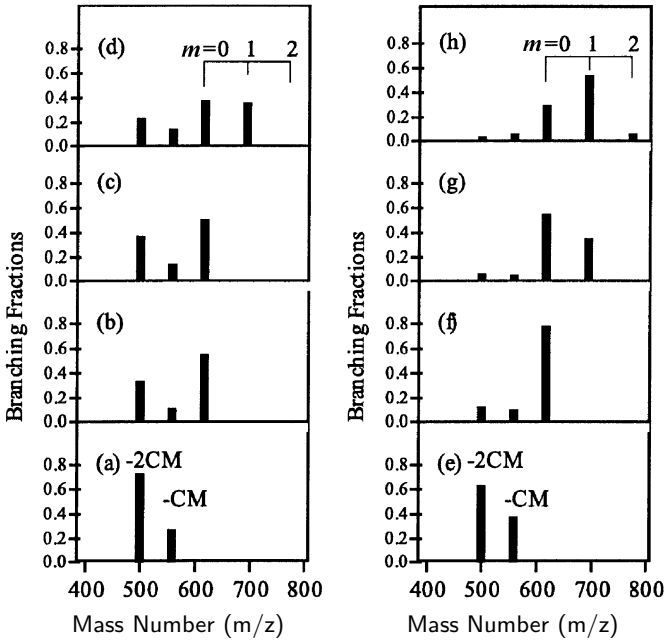

Fig. 1. Branching fractions of fragment ions produced by irradiation at 28200 cm^{-1} of hemin$^+$(DMSO)$_n$ ($n = 0$ (a) to 3 (d)), and at 18800 cm^{-1} ($n = 0$ (e) to 3 (h)) are plotted as filled bars, respectively. Cluster ions, hemin$^+$(DMSO)$_m$ ($0 \leq m < n$), and fragments of hemin$^+$ are observed as the product ions. Fragments of hemin$^+$, [hemin–CH_2COOH]$^+$ (558 amu) and [hemin–2(CH_2COOH)]$^+$ (499 amu), are indicated by symbols, –CM and –2CM, respectively.

3 Results and discussion

3.1 Photoreactions of hemin$^+$(DMSO)$_n$

Figure 1 shows the mass distributions of the fragment ions produced by the photolysis of hemin$^+$(DMSO)$_n$ ($n = 0$−3) clusters with the 2nd (18800 cm^{-1}) and 3rd harmonic (28200 cm^{-1}) of the YAG laser. Porphyrinic compounds show several absorption bands of moderate intensity in visible region, which are called as a Q band. In addition to these bands, an extremely strong absorption band is observed at ∼25000 cm^{-1}, which is called as a Soret band [16]. In porphyrins, highest-occupied molecular orbital (HOMO) and lowest-unoccupied molecular orbital (LUMO) are π-type orbitals; HOMO ($1a_{1u}$), next-HOMO ($3a_{2u}$), and degenerated LUMO ($4e_g$) are called as "four orbitals" and are well separated from the other orbitals. The Q and Soret bands are ascribed to the promotion of the electrons from the $1a_{1u}$ and $3a_{2u}$ orbitals to the $4e_g$ orbital, respectively: the Q and Soret bands correspond to the transitions to the $1E_u$ and $2E_u$ states, respectively [16]. The irradiations at 18800 and 28200 cm^{-1} correspond to the excitations of the $1E_u$ and $2E_u$ states, respectively. As shown in the figure, the fragment ions generated through the decomposition of hemin$^+$ ion are observed at 558 and 499 amu in addition to the evaporation products such as hemin$^+$(DMSO)$_m$ ($0 \leq m < n$). The product ions at 558 and 499 amu are assigned to the fragments, which loss one and/or two carboxymethyl groups, –CH_2COOH (59 amu), by the β-cleavage reaction, respectively. In Figure 1, the fragment ions with loss of one and two –CH_2COOH groups are designated as –CM and –2CM, respectively. With increasing the excitation energy from 18800 to 28200 cm^{-1}, the evaporation of DMSO and β-cleavage reaction are enhanced. Since we observe no indication of the reaction *via* an excited-state channel, the product ions are considered to be generated through the higher vibrational levels in the ground state repopulated *via* a fast internal conversion as follows; photoexcitation and repopulation of the higher vibrational levels of hemin$^+$ cluster ions in the ground state (Eq. (1)), subsequent sequential evaporation (Eq. (2)), and decomposition

of hemin$^+$ (Eqs. (3, 4));

$$\text{hemin}^+(\text{DMSO})_n + h\nu \rightarrow [\text{hemin}^+(\text{DMSO})_n]^* \rightarrow [\text{hemin}^+(\text{DMSO})_n]^\ddagger \quad (1)$$

$$[\text{hemin}^+(\text{DMSO})_n]^\ddagger \rightarrow \text{hemin}^+(\text{DMSO})_m + (n-m)\text{DMSO} \rightarrow ... \rightarrow \text{hemin}^+ + n\text{DMSO} \quad (m \leq n) \quad (2)$$

$$[\text{hemin}^+(\text{DMSO})_n]^\ddagger \rightarrow [\text{hemin}^+ - \text{CH}_2\text{COOH}](\text{DMSO})_n + \bullet\text{CH}_2\text{COOH}$$

$$[\text{hemin}^+ - \text{CH}_2\text{COOH}](\text{DMSO})_n \rightarrow ... \rightarrow \text{hemin}^+ - \text{CH}_2\text{COOH} + n\text{DMSO} \quad (3)$$

$$[\text{hemin}^+ - \text{CH}_2\text{COOH}](\text{DMSO})_n \rightarrow [\text{hemin}^+ - 2(\text{CH}_2\text{COOH})](\text{DMSO})_n + \bullet\text{CH}_2\text{COOH}$$

$$[\text{hemin}^+ - 2(\text{CH}_2\text{COOH})](\text{DMSO})_n \rightarrow ... \rightarrow \text{hemin}^+ - 2(\text{CH}_2\text{COOH}) + n\text{DMSO} \quad (4)$$

where $[\text{hemin}^+(\text{DMSO})_n]^*$ and $[\text{hemin}^+(\text{DMSO})_n]^\ddagger$ represent the clusters in the initially excited state and the higher vibrational state on the ground-state surface, respectively. In the present study, solvated product ions such as $[\text{hemin}^+\text{-}k(\text{CH}_2\text{COOH})]\,(\text{DMSO})_m$ ($k = 1$ or 2, $m \leq n$) are not observed. This result seems to indicate that both the evaporation and β-cleavage reaction may take place competitively from the higher vibrational levels of the electronic ground state.

3.2 Photoionization of cytochrome c ions

Multiply-charged cytochrome c ions, $(\text{M} + n\text{H})^{n+}$ ($n = 9$ to 17), are produced by ESI. The photo-induced reactions of the charge-state selected cytochrome c ions are investigated at 18800 and 28200 cm^{-1}. All charge states examined exhibit relatively strong photodepletion in both excitations. The absorption bands in visible and UV regions of cytochrome c in solution are ascribed to the $\pi\pi^*$ transition of heme. The photo-induced reactions of the ions are examined by the excitation of these transitions in heme. The product ions are considered to be generated through the following processes; photoexcitation of heme in the protein ions, subsequent photoionization to produce $(\text{M}+n\text{H})^{(n+1)+}$, or photodissociation. In this scheme, the photoionization competes with the dissociation. A number of fragments have been observed *via* the cleavage of polypeptide chains in the collision-induced dissociation (CID) of protein ions [18]. We would also expect to observe the similar fragmentation process for the photolysis of protein ions. In contradiction with this expectation, the fragment ions are not detected with sufficient intensity except for the multiply-charged ions, $(\text{M} + n\text{H})^{(n+1)+}$.

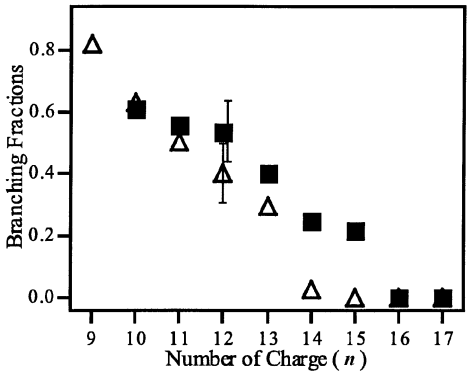

Fig. 2. Branching fractions for the photoionization of multiply-charged cytochrome c ions plotted as a function of charge. Open triangles and filled squares show the branching fractions at 18800 cm^{-1} and 28200 cm^{-1}, respectively.

In order to analyze the photodissociation process, we examine the branching fraction for the ionization, R_{ion}, which is defined as

$$R_{ion} = I_{pro}\left[(\text{M} + n\text{H})^{(n+1)+}\right] / I_{dep}\left[(\text{M} + n\text{H})^{n+}\right] \quad (5)$$

where $I_{pro}[(\text{M} + n\text{H})^{(n+1)+}]$ is the ion intensity of the product ion, $(\text{M} + n\text{H})^{(n+1)+}$, whereas $I_{dep}[(\text{M} + n\text{H})^{n+}]$ is the depletion ratio of the parent ion. Figure 2 shows the branching fractions of the photoionization process plotted as a function of charge, n. Open triangles and filled squares indicate the branching fractions determined at 18800 (47 mJ cm^{-2} pulse^{-1}) and 28200 cm^{-1} (7.8 mJ cm^{-2} pulse^{-1}), respectively. As shown in the figure, the branching fractions in both excitations decrease monotonously with increasing the charge up to $n = 16$. The branching fractions are not dependent on the laser fluence in both excitations. The laser fluence dependence on the photodepletion yield is examined at 28200 cm^{-1}. The depletion yield increases in proportion to the 2.2 power of the laser fluence; the reactions proceed *via* two-photon excitation. The photodepletion yield at 18800 cm^{-1} also increases in proportion to the 2∼3 power of the laser fluence. The ionization cross sections from the $\pi\pi^*$ excited states are assumed to be the same as that for the transition from the ground state. The rate constants for the ionization from the excited states are estimated as 3.0×10^{11} s^{-1} and 2.0×10^{11} s^{-1} at 28200 cm^{-1} and 18800 cm^{-1}, respectively. Lifetime of the $\pi\pi^*$ excited state of iron porphyrins in solution has been reported as 25−50 ps [19]. The rate constants of the ionization are nearly the same order as that of the decay process. Therefore, the observed photoionization of cytochrome c ions is ascribed to the multiphoton excitation of heme.

As mentioned previously, the photoionization at 28200 cm^{-1} proceeds *via* two-photon excitation of heme for $n < 16$. In order to clarify the origin of the size-dependence of the photoionization yield, we carry out the model calculations. Since the polypeptide in cytochrome c ions has positive charges, the photo-ejection of an electron (ionization) from heme takes place under the influence of

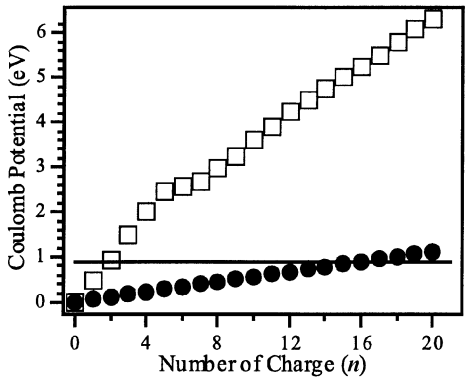

Fig. 3. Coulomb attractive potentials at heme, which arise from the charges on the linear polypeptide chain, are plotted with filled circles. The Coulomb potentials arisen from the charges on the surface of the sphere, are also plotted with open squares. The solid line indicates the excess energy, E_{ex}, of two-photon ionization at 28200 cm^{-1}.

Coulombic attractive potential. In a crude approximation, the upper limit of the excess energy, E_{ex}, in the photoionization can be defined as

$$E_{ex} = 2h\nu - \mathrm{IP}_{\mathrm{heme}} \tag{6}$$

where $h\nu$ and $\mathrm{IP}_{\mathrm{heme}}$ are the photon energy and the ionization potential (IP) of heme in cytochrome c ions. The photoionization may occur if the attractive potential becomes less than E_{ex}. Ionization potential of the gas-phase iron-porphyrins has been determined to be 6.06−6.09 eV [20, 21]. Thus, E_{ex} in the two-photon ionization at 28200 cm^{-1} (6.99 eV) is estimated to be ∼0.9 eV.

In the first scheme, the Coulomb attractive potential is estimated by assuming that the shapes of the protein ions are spheres. It is also assumed that the charges are distributed uniformly over the surface of the sphere. Jarrold and coworkers have examined the cross-sections of cytochrome c ions in the gas phase as a function of charge by ion mobility measurements [12,13]. Using these values, the Coulomb potential energy on the surface of the sphere is calculated. The values are plotted in Figure 3 as open squares as a function of n. The value is calculated to be 5.2 eV for $n = 16$, which is larger than E_{ex}. This result suggests that the Coulomb potential energy is overestimated with this model. Therefore, the arguments suggest that the conformation is quite different from sphere.

The molecular dynamics simulations for cytochrome c ions have predicted that cytochrome c ions in the present experiments ($n = 9$−17) are completely unfolded [12,13]. Heme is covalently bound to two cysteines. In native conformation, heme iron is bound to histidine and methionine. When cytochrome c unfolds, these ligands would dissociate from the iron. Thus, in the second model, the Coulomb attractive potential is estimated by assuming that the polypeptide chain in the protein ions is a linear string, and that the charges are distributed uniformly over the polypeptide chain. The calculated Coulomb potentials are plotted in Figure 3 as filled circles. The value for $n = 16$ is given as 0.89 eV and is almost equal to the excess energy, E_{ex}. For $n < 16$, the Coulomb potentials become lower than E_{ex} and the ionization is expected to occur. These results are consistent with the present experimental findings; the critical number of charge, n, for the ionization is 16. Therefore, the calculations indicate that the shapes of the protein ions are similar to the linear string. Although the present calculations use the oversimplified models, the results are consistent with the observed behaviors for the photoionization of cytochrome c ion.

This work is partially supported by the Grant-in-Aid (Grants #11304042) from the Ministry of Education, Science, Sports and Culture of Japan, and by the Grant-in-Aid for Scientific Research (Grants #11740326, and #13640512) and a research grant for the future program from Japan Society for Promotion of Science. KF is also grateful to the Hyogo Science and Technology Association for partial financial supports.

References

1. *Clusters of Atoms and Molecules*, edited by H. Haberland (Springer-Verlag, Heidelberg, 1994), Vols. I and II, and references cited therein
2. K. Fuke, K. Hashimoto, S. Iwata, Adv. Chem. Phys. **110**, 431 (1999), and references cited therein
3. Y. Ohshima, O. Kajimoto, K. Fuke, *Electron Transfer in Chemistry*, edited by Y. Haas (Wiley-VCH, 2001)
4. P. Brockhaus, I.V. Hertel, C.P. Schulz, J. Chem. Phys. **110**, 393 (1999)
5. *Electrospray Ionization Mass Spectrometry*, edited by R.B. Cole (Wiley, New York, 1997)
6. T.G. Spence, T.D. Burns, G.B. Guckenberger, L.A. Posey, J. Phys. Chem. **101**, 1081 (1997)
7. C.J. Thompson, J. Husband, F. Aguirre, R.B. Metz, J. Phys. Chem. **104**, 8155 (2000)
8. X.-B. Wang, L.-S. Wang, J. Chem. Phys. **111**, 4497 (1999)
9. *The Porphyrin handbook*, edited by K.M. Kadish, K.M. Smith, R. Guilard (Academic Press, San Diego, 2000), and references cited therein
10. R.A. Zubarev, D.M. Horn, E.K. Fridriksson, N.L. Kelleher, N.A. Kruger, M.A. Lewis, B.K. Carpenter, F.W. McLafferty, Anal. Chem. **72**, 563 (2000)
11. R.A. Jockusch, P.D. Schnier, W.D. Price, E.F. Srittmatter, P.A. Demirev, R. Williams, Anal. Chem. **69**, 1119 (1997)
12. M.F. Jarrold, Acc. Chem. Res. **32**, 360 (1999)
13. Y. Mao, M.A. Ratner, M.F. Jarrold, J. Am. Chem. Soc. **123**, 6503 (2001)
14. S. Nonose, H. Tanaka, K. Fuke, Int. J. Mass Spetrom. (submitted)
15. S. Nonose, H. Tanaka, N. Okai, T. Shibakusa, K. Fuke, Eur. Phys. J. D **20**, 619 (2002)
16. M. Gouterman, J. Mol. Spectrosc. **6**, 138 (1961)
17. H. Budzikiewicz, *The Porphyrins*, edited by D. Dolphin (Academic Press, New York, 1978), Vol. III, pp. 395-459
18. R.D. Smith, C.J. Barinaga, H.R. Udseth, J. Phys. Chem. **93**, 5019 (1989)
19. K. Kalyanasundaram, *Photochemistry of Polypyridine and Porphyrin Complexes* (Academic Press, London, 1992), pp. 493-534
20. S. Kitagawa, I. Morishima, T. Yonezawa, N. Sato, Inorg. Chem. **18**, 1349 (1979)
21. Y. Nakato, K. Abe, H. Tsubomura, Chem. Phys. Lett. **39**, 358 (1976)